

Practical Methods for Distance-Adaptive Continuous-Variable Quantum Key Distribution

Jonas Berl, *Graduate Student Member, IEEE*, Utku Akin, *Graduate Student Member, IEEE*,
Erdem Eray Cil, *Graduate Student Member, IEEE*, Laurent Schmalen, *Fellow, IEEE*,
and Tobias Fehenberger, *Member, IEEE*

Abstract—Continuous-variable quantum key distribution (CV-QKD) is a promising quantum-safe alternative to classical asymmetric cryptography that enables two authenticated parties to establish a shared secret over a potentially eavesdropped quantum channel. A key step in CV-QKD post-processing is information reconciliation, which leverages forward error correction (FEC) techniques to extract identical bit strings from noisy correlated data. In this work, we analyze the strict limitations on operating distance that are imposed by constant-rate FEC, severely limiting the practicability of CV-QKD systems in deployed optical networks. To overcome the distance limitations, we evaluate three strategies: (i) tuning modulation variance, (ii) adding controlled amounts of trusted detector loss, and (iii) the use of rate-adaptive FEC. All approaches are validated experimentally, compared in terms of performance, and we discuss implementation aspects. Our results show that while methods (i) and (ii) extend the operational distance of constant-rate FEC without the need for additional hardware components, they incur a significant penalty in secret key rate (SKR). In contrast, rate-adaptive FEC enables CV-QKD operation with performance close to the asymptotic SKR over a wide range of distances, provided that the reconciliation efficiency is chosen appropriately.

Index Terms—CV-QKD, information reconciliation, distance-adaptivity, secret key rate

I. INTRODUCTION

IN recent years, quantum computing has seen remarkable advances [2]–[4], posing a significant threat to secure communication in the foreseeable future. With Shor’s algorithm and cryptographically-relevant quantum computing, asymmetric schemes such as Rivest–Shamir–Adleman (RSA), the Diffie-Hellman-Merkle key agreement or elliptic curve cryptography are at high risk [5], [6]. As a result, attention has

shifted to quantum-safe cryptographic schemes, such as post-quantum cryptography (PQC) and quantum key distribution (QKD). While PQC is an algorithmic solution and is therefore still susceptible to future advances in mathematics and quantum computing, QKD offers the potential for information-theoretic security [7].

Since its introduction by Bennett and Brassard in 1984 [8], QKD has seen significant development with the first commercial systems available as of today. QKD is a method for *key distribution*, i.e., it is meant to establish a shared secret key between two authenticated parties, typically connected by an optical fiber or a free space optical link. There are two main types of QKD. In discrete-variable quantum key distribution (DV-QKD), the transmitting side, often called Alice, encodes random information on discrete variables of a quantum state, e.g., on the polarization of single photons, and sends the states to the receiving side, typically named Bob [7]. The other type is continuous-variable quantum key distribution (CV-QKD), where Alice encodes the information on continuous variables of a coherent state, e.g., in the quadratures of an electromagnetic field emitted by a laser [9]. The security of both methods is based on quantum mechanical principles, such as the no-cloning theorem and the uncertainty principle [10]. These forbid a potential eavesdropper, Eve, from obtaining a (partial) copy of the transmitted information without being detected. Due to its compatibility with commercial off-the-shelf components and photonic miniaturization [11]–[13], CV-QKD is regarded as a cost-effective alternative to DV-QKD. However, CV-QKD comes with more challenges in post-processing, with the error correction step, commonly referred to as information reconciliation (IR), being particularly more demanding.

In experimental investigations of CV-QKD, the emphasis is typically placed on physical layer effects, whereas the influence of post-processing on the secret key rate (SKR) is frequently not taken into account. For example, the reconciliation efficiency and frame error rate (FER) are often treated as constant values and little justification is provided for the specific choices made [14]–[17]. In practice, however, both parameters change with the channel loss, are susceptible to temporal variations of channel conditions, and depend on the characteristics of the employed forward error correction (FEC). Besides an inaccurate estimation of the SKR, the effects of distance-dependent FER and reconciliation efficiency also cause strict distance limitations. For operators that expect QKD systems to function reliably over a wide range of

This work is partially funded by the German Federal Ministry of Research, Technology and Space under the project DE-QOR (Grant IDs 16KISQ052K and 16KISQ056) and SEQUIN (Grant ID 16KIS2132K). This article was presented in part at the European Conference on Optical Communication (ECOC), Frankfurt, Germany, September 2024 [1]. (Corresponding author: Jonas Berl (jonas.berl@advasecurity.com))

Jonas Berl, Utku Akin and Tobias Fehenberger are with Adva Network Security GmbH, Fraunhoferstraße 5, Martinsried/Munich, Germany.

Jonas Berl, Erdem Eray Cil and Laurent Schmalen are with the Communications Engineering Lab, Karlsruhe Institute of Technology, Hertzstraße 16, Karlsruhe, Germany.

Utku Akin is with the Institute for Communications Engineering, Technical University of Munich, Theresienstraße 90, Munich, Germany.

Article DOI: 10.1109/JLT.2026.3664474

© 2026 IEEE. Personal use of this material is permitted. Permission from IEEE must be obtained for all other uses, in any current or future media, including reprinting/republishing this material for advertising or promotional purposes, creating new collective works, for resale or redistribution to servers or lists, or reuse of any copyrighted component of this work in other works.

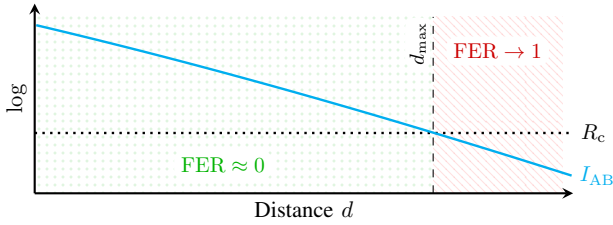


Fig. 1. Error correction for classical communications: mutual information I_{AB} and constant code rate R_c over the distance d for a constant modulation variance.

distances, distance-adaptive CV-QKD solutions are therefore of particular interest.

Recent research has examined the influence of practical reconciliation on system performance, especially addressing the resulting distance limitations. For instance, it has been demonstrated that an optimization of the modulation variance can support CV-QKD over a broad range of distances, even when only a limited number of constant-rate FEC codes are available [18]–[20]. Similarly, the controlled injection of trusted detector noise has been investigated numerically to match the FEC code rate and received signal-to-noise ratio (SNR), outperforming alternative techniques for rate-adaption such as shortening and puncturing [21]. As another option, rate-adaptive FEC techniques, e.g., based on Raptor codes and Raptor-like low-density parity-check (RL-LDPC) codes, have been proposed. For example, simulations with Raptor codes show that joint optimization of modulation variance and rate-adaptive FEC can yield high reconciliation efficiencies and positive SKRs over a wide range of transmission distances [22]. To address small-scale channel fluctuations, the combination of controlled amounts of trusted detector noise and a rate-adaptive FEC code has been shown effective for codes with step-wise rate adaption [23]. Nonetheless, most of these approaches have not yet been validated by experiments, and a comprehensive comparison of these methods is missing.

In this paper, we illustrate the impact of practical reconciliation on CV-QKD system performance, focusing on the imposed distance limitations. We validate our findings experimentally and investigate three practical strategies to achieve distance-adaptive operation. The first method relies on tuning the modulation variance, so that the received SNR is matched to the rate of the available FEC code, enabling a single constant-rate FEC code to be used across a broad range of distances. The second approach leverages the trusted-device scenario, where deliberately adding a controlled amount of trusted detector loss can be used to similarly adjust the received SNR for distance-adaptive operation. As third strategy, we consider rate-adaptive FEC, where the code rate used during IR can be adapted to the transmission distance. We demonstrate all investigated methods experimentally, compare their performance, and discuss implementation aspects.

II. DISTANCE-ADAPTIVE RECONCILIATION

The main performance metric of any QKD system is the SKR as a function of distance. Considering reverse reconcili-

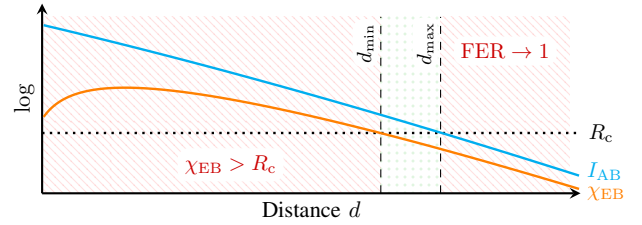


Fig. 2. IR for CV-QKD: mutual information I_{AB} , Holevo bound χ_{EB} and constant code rate R_c over the distance d for a constant modulation variance.

ation, the asymptotic SKR is computed as [9]

$$\text{SKR} = \beta I_{AB} - \chi_{EB}, \quad (1)$$

where I_{AB} is the mutual information between Alice and Bob, χ_{EB} is the Holevo bound between Eve and Bob, and β denotes the reconciliation efficiency. When IR is implemented with FEC, the reconciliation efficiency needs to be replaced by the multiplicative gap between code rate R_c and mutual information, i.e., $\beta = R_c/I_{AB}$. We denote this updated key rate as *extracted SKR*. Accounting for erroneous frames, the asymptotic extracted SKR is formulated as [9]

$$\text{SKR} = (1 - \text{FER})(R_c - \chi_{EB}). \quad (2)$$

Here, we neglect other scaling factors, such as the fraction of quantum states used for parameter estimation or idle times during calibration. Equation (2) helps explain the fundamental difference between error correction in classical communications and the impact of practical IR on the extracted SKR.

According to the channel coding theorem, there exist error-correcting codes with decoder that allow an arbitrarily small error probability as long as the code rate R_c is smaller than the channel capacity (or equivalently the applicable mutual information) [24]. To illustrate the effect of constant-rate FEC, we consider the mutual information I_{AB} of the symbols transmitted over the quantum channel between Alice and Bob. For heterodyne detection, it is computed as [9]

$$I_{AB} = \log_2 \left(1 + \frac{TV_{\text{mod}}}{2 + \xi} \right), \quad (3)$$

where T is the effective transmittance and includes both the channel and detector transmittance, T_{ch} and T_{det} , respectively. The modulation variance is denoted as V_{mod} and ξ is the excess noise, both of which are typically normalized to the shot noise unit (SNU).

In Fig. 1, we present a qualitative curve of mutual information as a function of the transmission distance, assuming a constant modulation variance and an infinitely steep FER degradation at channel capacity (i.e., we model the FER as a Heaviside step function). The arbitrary but fixed code rate R_c of the FEC code used during IR is depicted by the dotted horizontal line. The channel attenuation is assumed to be $T_{\text{ch}} = 10^{-\alpha d}$, where α is the fiber attenuation in dB/km. As shown, as long as the mutual information is larger than the fixed code rate, codewords can be decoded successfully and the FER is approximately zero. When the code rate becomes larger than the mutual information, codewords can

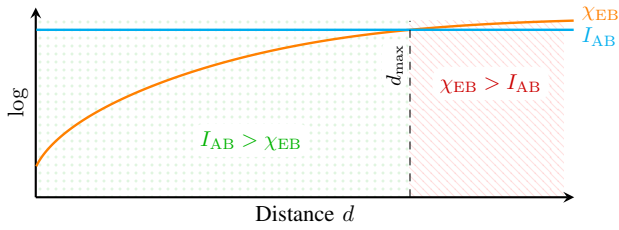


Fig. 3. Mutual information I_{AB} and Holevo bound χ_{EB} over the distance d when the modulation variance is tuned for constant received SNR.

no longer be decoded, resulting in an FER that approaches one. Therefore, the error correction step introduces an upper bound on the operating distance marked by the vertical dashed line at d_{\max} . Beyond this distance, the correlated noisy data of Alice and Bob can no longer be reconciled.

For CV-QKD as stated in (2), two conditions must be fulfilled for a positive extracted SKR. First, at least one FEC frame must be decoded successfully, which implies an FER of less than one. Similarly to the upper bound on operating distance for classical communications, the error correction step limits the reach of the system. Second and unique to CV-QKD, the rate of the employed FEC code must be larger than the Holevo bound. Otherwise, Eve obtains more information on the raw key material than Alice and Bob, and the protocol must be aborted. Due to the course of the Holevo bound shown in Fig. 2, this condition is not fulfilled up to a minimum distance d_{\min} , marked by the left vertical dashed line. Hence, only a small window of consecutive distances of width $\Delta d = d_{\max} - d_{\min}$ can be covered with a single constant-rate FEC code. Moreover, as the difference $I_{AB} - \chi_{EB}$ becomes smaller over distance, FEC codes with increasingly higher reconciliation efficiencies are required to extract secrecy in long-distance scenarios.

The distance limitations of constant-rate FEC pose severe practical challenges during the integration of CV-QKD into existing telecommunication infrastructure as operators expect systems to function reliably over a wide range of distances. Trivially, a potentially large set of FEC codes, i.e., one for each targeted distance window, can be used to overcome the distance limitations. We refer to this strategy as method ① and examine three alternative strategies in the following, summarized in Tab. I.

In method ①, the modulation variance is tuned for distance-adaptive operation [18], [19]. For this approach, we assume access to a single FEC code with fixed rate R_c . Adjusting the modulation variance scales the signal power and thereby influences both the received SNR and the Holevo bound. By maintaining a constant SNR at Bob’s receiver, independent of channel transmittance, the FER condition in (2) can be satisfied. In Fig. 3, we depict the mutual information (or equivalently code rate) and Holevo bound qualitatively, scaling the modulation variance for a constant received SNR. As shown, there no longer is a lower limit on operational distance and the mutual information remains larger than the Holevo bound up to the maximum reach of the system marked by the dashed vertical line at d_{\max} .

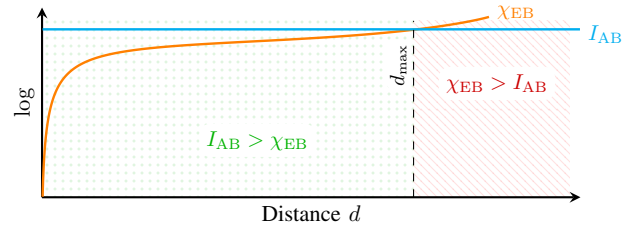


Fig. 4. Mutual information I_{AB} and Holevo bound χ_{EB} over the distance d when the trusted detector loss is scaled for constant received SNR.

TABLE I
SUMMARY OF INVESTIGATED METHODS FOR DISTANCE-ADAPTIVE CV-QKD

Method	Description
Method ① (trivial)	Set of constant-rate FEC codes
Method ①	Single constant-rate FEC code with tuned modulation variance
Method ②	Single constant-rate FEC code with adding controlled amounts of trusted detector loss
Method ③	Rate-adaptive FEC code

The second strategy ② leverages the trusted-device scenario, in which the trusted parts of transmittance and excess noise, e.g., the inherent detector loss, are not attributed to an attacker during the computation of the SKR [9]. In this case, the receiver can deliberately add trusted noise, trusted loss or a combination of both to match the received SNR to the rate of the available FEC code [21], [25]. Similarly to method ①, we assume access to a single FEC code with rate R_c and focus on trusted loss as this can be implemented with a variable optical attenuator (VOA) at Bob’s input. Again, changing the trusted detector loss has an impact on the received SNR and the Holevo bound. It should be noted that although both tuning the modulation variance and adding trusted loss have the same effect on the received SNR, their impact on the Holevo bound and consequently the SKR differs, as illustrated in Fig. 4. This difference arises because the Holevo bound is computed as the difference between two entropies: the von Neumann entropy of the state accessible to Eve and the von Neumann entropy of the same state after Bob has performed his measurement [9]. While tuning the modulation variance affects both entropies, adjusting the trusted detector loss only has an effect on the latter.

As a third approach ③, we investigate the use of rate-adaptive FEC, with an emphasis on RL-LDPC codes that have recently attracted interest in CV-QKD [26], [27]. RL-LDPC codes are designed by first constructing a parity-check matrix for a high-rate code and then extending it to lower rates through the incremental addition of degree-1 parity bits with optimized connectivity. Compared to conventional methods for rate-adaptivity, such as puncturing or shortening, this approach yields superior performance across the low code rate regime typically considered for CV-QKD [28]. During encoding, the number of added degree-1 parity bits is chosen according to the desired code rate. These bits are generated based on pre-optimized connections and are appended to the high rate

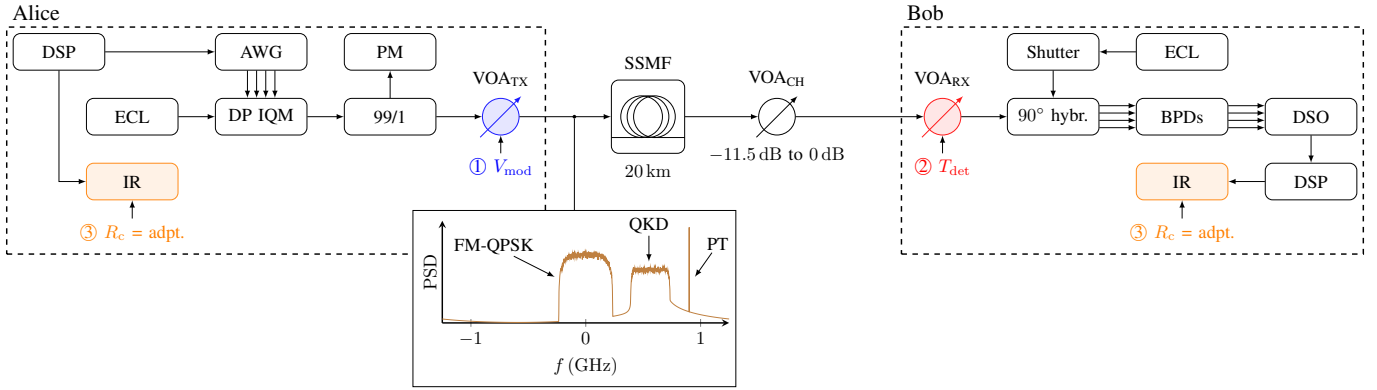


Fig. 5. Experimental setup for distance-adaptive CV-QKD. The investigated approaches ① to ③ are colored in blue, red and orange. The inset shows a qualitative plot of the power spectral density (PSD) of the transmit signal, consisting of FM-QPSK, QKD and the digital PT.

code word, thereby reducing the effective rate. Decoding is done on a specific part of the graph representation of the code matching the lowest code rate, while the selection of the subgraph is determined by the target code rate. This approach allows for a single decoder design capable of supporting multiple code rates, eliminating the need for distinct hardware implementations.

III. EXPERIMENTAL SETUP

The CV-QKD system under study is depicted in Fig. 5. The transmitter consists of an offline digital signal processing (DSP) block which generates an eight-fold oversampled probabilistic-shaped (PS)-256QAM transmit sequence with a symbol rate of 312.5 MBd and a block length of 2^{19} quantum states. Experimentally, the use of higher-order PS-QAM has been shown to sufficiently approximate Gaussian modulation and achieve high SKRs while staying compatible with practical equipment [29]. To facilitate clock recovery and I/Q skew compensation on Bob's side, a frequency-multiplexed QPSK (FM-QPSK) signal is added, while polarization demultiplexing and carrier recovery are facilitated by an additional digital pilot-tone (PT) [30]–[32]. Both signals are known by the receiver and their power level relative to the QKD signal is defined as pilot-to-signal power ratio (PSPR), i.e.,

$$\text{PSPR} = \frac{P_{\text{FM-QPSK}} + P_{\text{PT}}}{P_{\text{QKD}}}, \quad (4)$$

where $P_{\text{FM-QPSK}}$ denotes the signal power of the FM-QPSK signal, P_{PT} is the power of the digital pilot and P_{QKD} is the power of the QKD signal. We use an external cavity laser (ECL) tuned to 1550 nm with a spectral line width of less than 2 kHz and a constant optical output power of 13 dBm. The transmit sequence consisting of QKD, FM-QPSK and digital pilot is generated with an arbitrary waveform generator (AWG) at a sampling rate of 2.5 GHz, while the electro-optical conversion happens in a dual-polarization I/Q-modulator (DP IQM). To monitor the power of the QKD signal continuously, we utilize a 99/1 splitter and measure 1% of the incident power with an optical power meter (PM). Since the transmit signal is generated in the high-power regime, we use the measured optical power and VOA_{TX} to ensure a constant

TABLE II
PARAMETERS OF THE EXPERIMENTAL SETUP

Parameter	Value
Symbol rate	312.5 MBd
Block length	2^{19}
Modulation format	PS-256 QAM
Laser wavelength	1550 nm
Laser linewidth	≤ 2 kHz
Laser power	13 dBm
Modulation variance	5 SNU
VOA_{CH} attenuation	-11.5 dB to 0 dB
DSO sampling rate	2.5 GHz
AWG sampling rate	2.5 GHz
FER threshold	10^{-2}

modulation variance of 5 SNU throughout all experimental protocol runs.

The quantum channel between Alice and Bob consists of 20 km standard single mode fiber (SSMF) and VOA_{CH} . Given the low signal powers employed in the experimental setup, effects from fiber non-linearity are negligible. In addition, linear transmission impairments, including chromatic dispersion and polarization-mode dispersion, have no significant impact on the signal at the low symbol rate, and are therefore not mitigated in DSP. Due to the stabilized experimental environment, state-of-polarization rotations remain largely static and are effectively compensated in DSP. The attenuation of VOA_{CH} can therefore be mapped to an equivalent SSMF distance, illustrating operation beyond 20 km.

On the receiving side, the signal enters another VOA that is used in method ② to control the trusted detector loss, while additionally functioning as a shutter during the calibration procedure. We denote this VOA as VOA_{RX} in the following and configure 0 dB attenuation during the experiments. After passing through the optical 90° hybrid and the four balanced photo diodes (BPDs), the signal is captured with a digital sampling oscilloscope (DSO) at a sampling rate of 2.5 GHz. The laser used for the local-local oscillator (LLO)¹ on Bob's side is tuned to 1550 nm and paired with Alice's transmit laser

¹Early CV-QKD systems transmitted the local oscillator (LO) along the quantum signal from Alice to Bob. To emphasize that the LO is generated on Bob's side, the term *local-local* oscillator is used.

to minimize the carrier frequency offset between both lasers. Additionally, the LLO can be cut-off using a polarization-maintaining shutter during calibration. The sampled signal is processed by offline DSP, making use of the FM-QPSK signal and digital PT embedded in the signaling scheme. We calibrate the QKD system before each quantum transmission to minimize the effect of systematic deviations between calibration and quantum transmission as described in [9]. Both parties share the block for IR. We follow the common assumption that Alice's and Bob's devices are trusted, i.e., an attacker cannot influence the device internals, marked by the dashed boundaries in Fig. 5. All experimental parameters are summarized in Tab. II.

A. Emulating SSMF Distance

To study the effects of varying operating distances, we sweep the channel loss using VOA_{CH} in 0.5 dB steps while the configuration of VOA_{TX} and VOA_{RX} remains unchanged. For each attenuation setting of VOA_{CH} , we record approximately 50 protocol runs. Sweeping the channel loss from -11.5 dB to 0 dB, this totals to around 1200 recorded protocol runs. After removing the runs in which the DSP failed to correctly estimate the I/Q skew or in which the received SNR falls outside the expected range, we are left with 864 protocol runs. To facilitate a fair comparison using the same protocol runs, we introduce the concept of *emulated* transmission distances, i.e., the fiber distance to which the current channel attenuation corresponds to. Given that the signal powers employed in CV-QKD, including the two helper signals, are well below the regime in which effects from fiber non-linearity become relevant, the quantum channel can be modeled as a *block-wise* linear time-invariant (LTI) system. The effects from long-term component drifts, such as laser power or VOA attenuation, are accounted for through the periodic calibration of the experimental setup at the beginning of each protocol run. Short-term time-varying effects from components can be partially compensated by DSP. For instance, polarization rotations are monitored and mitigated by an adaptive equalizer while clock deviations between AWG and DSO are resolved using interpolation. This simplification permits re-distributing the transmittance of VOA_{CH} between the three employed VOAs *after* the measurement run. While Bob's received waveform remains unchanged, the computation of the Holevo bound and, consequently, the SKR are affected. Under the trusted-device assumption, part of the channel loss is then attributed to the trusted detector or to a change in modulation variance rather than to a potential attacker.

To investigate methods ① and ②, we first group the recorded measurements according to their VOA_{CH} setting. After removing failed DSP runs and considering only protocol runs with positive excess noise, the received SNR for the considered group of measurements is approximately constant. In the next step, we re-distribute the constant loss of VOA_{CH} to either VOA_{TX} or VOA_{RX} to emulate changes in distance. To that end, we compute a vector of emulated channel transmittance, taking into account distances d from 0 km to 100 km and assuming a fiber attenuation of $\alpha = 0.2$ dB/km.

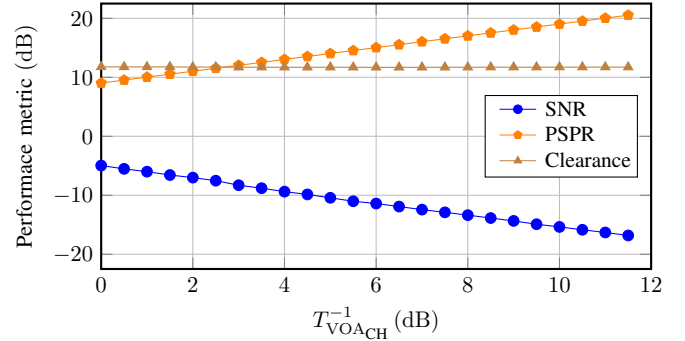


Fig. 6. Experimental results for mean SNR, the configured PSPR and mean clearance as a function of VOA_{CH} attenuation.

Given the measured channel transmittance for a particular setting of VOA_{CH} , we determine the baseline, i.e., the true channel attenuation of the current experimental setup. This is important since the insertion loss of VOA_{CH} and the true attenuation of the 20 km SSMF fiber spool must be considered. For method ①, the baseline modulation variance is $V_{\text{mod}} = 5$ SNU. If more or less distance should be emulated for a given VOA_{CH} setting, then the emulated modulation variance needs to be adjusted according to

$$V_{\text{mod}}^{\text{emul}} = V_{\text{mod}} T_{\text{VOA}_{\text{CH}}} / T_{\text{FL}}, \quad (5)$$

where $T_{\text{VOA}_{\text{CH}}}$ denotes the transmittance of VOA_{CH} and $T_{\text{FL}} = 10^{-\alpha d}$ is the emulated fiber loss. Similarly, the emulated attenuation can be re-distributed to VOA_{RX} and be taken into account as trusted detector loss during SKR computation. For method ②, the detector transmittance is updated as

$$T_{\text{det}}^{\text{emul}} = T_{\text{det}} T_{\text{VOA}_{\text{CH}}} / T_{\text{FL}}, \quad (6)$$

where $T_{\text{det}}^{\text{emul}} \in [0, T_{\text{det}}]$. Notably, the modulation variance can be chosen freely (within experimentally viable ranges) in method ① while the actual trusted detector loss serves as an upper bound on the emulated loss in method ②. At the same time, this is also an upper bound on the achievable (emulated) transmission distance.

B. Experimental Findings

As shown in Fig. 6, the experimental setup operates in the shot-noise limited regime, exhibiting an average clearance of 11.7 dB across all protocol runs. Following the convention in the literature, we compute the clearance as the ratio of shot noise to electronic noise variance, evaluated over the QKD signal bandwidth [9]. Moreover, we find that the received SNR follows the VOA_{CH} attenuation linearly. The consistent behavior of SNR and clearance across different VOA_{CH} configurations empirically supports the block-wise LTI assumption, indicating that time-varying effects from components are negligible. To help the receiver DSP, we keep the pilot power at the input of the receiver constant by scaling the PSPR with the channel loss. In Fig. 7, we present the measured excess noise ξ over the VOA_{CH} attenuation, which shows the expected exponential decay over the channel transmittance. It includes, for instance, noise due to non-ideal

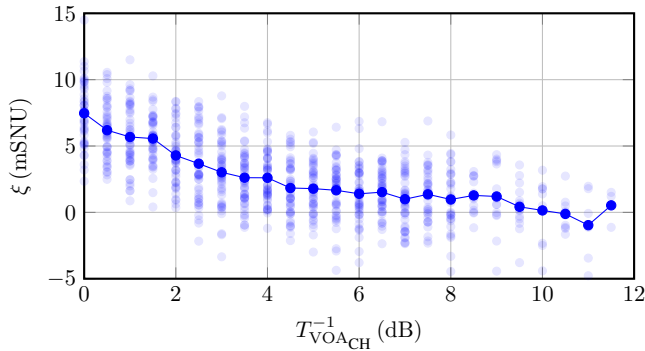


Fig. 7. Experimental results for excess noise ξ over the VOA_{CH} attenuation, considering protocol runs with non-failing DSP only. The means for each VOA_{CH} attenuation setting are indicated with solid markers. We report excess noise at the channel output.

state preparation at the transmitter, such as thermal noise in the transmitter electronics. At the discrete receiver, fiber length mismatches in the eight arms of the polarization-diverse optical hybrid constitute an additional impairment that cannot be mitigated by DSP and that adds to the measured excess noise. Moreover, DSP implementation imperfections, e.g., an inaccurate estimation and compensation of carrier frequency or clock offset, further contribute to the measured excess noise. Because of statistical fluctuations, some protocol runs yield negative estimates of the excess noise. Additionally, the total number of valid protocol runs decreases as channel attenuation increases, since the DSP fails more frequently under the more challenging conditions.

C. Information Reconciliation

We employ an open-source implementation of multidimensional reconciliation [33] based on a rate-adaptive RL-LDPC code [28], [34]. Its rate can be adjusted between 0.01 and 0.2, and the block length ranges from 10^5 bit to 2×10^6 bit. Eight-dimensional reconciliation is adopted, as it offers the best performance [35] while maintaining low computational complexity due to the Cayley-Dickson construction [36]. Decoding is performed using the iterative sum-product algorithm, with the maximum number of iterations set to 150. To synthetically increase the number of available states for a protocol run, we iteratively permute and shuffle the recorded quantum states until 100 erroneous frames are observed for each protocol run. This approach is necessary because the number of FEC frames generated from a single protocol run is too small to yield statistically significant results. In addition, especially for low code rates, the block length may even exceed the number of quantum states that are recorded in a single protocol run.

D. Post-processing

As the considered experimental setup is modeled as a block-wise LTI system, re-distributing the attenuation between the employed VOAs has no impact on Bob's received waveform and on the IR phase in general. We conduct IR for all protocol runs with four constant code rates and four different settings for the reconciliation efficiency using the RL-LDPC code,

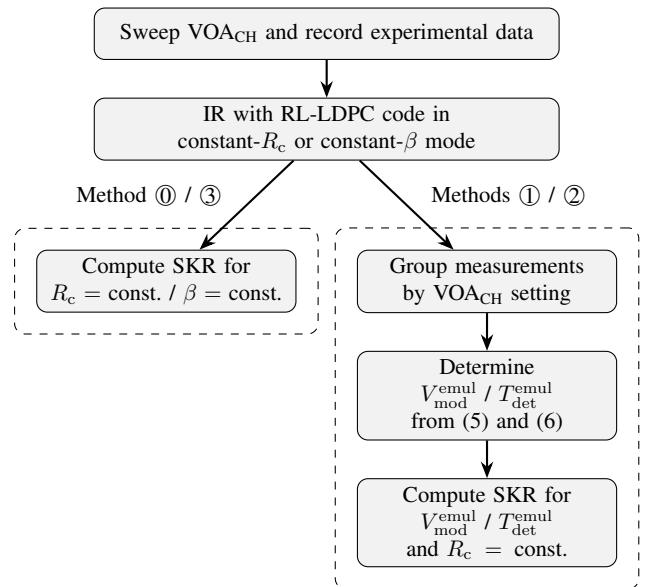


Fig. 8. Post-processing of experimental data for methods ① to ③.

either in constant-rate or constant reconciliation efficiency mode. For the latter, we compute the code rate with the help of (3) and the SNR estimated after DSP. With the obtained statistics, we determine the extracted SKR as a function of the emulated distance. Since higher-order PS-QAM has been reported to closely resemble Gaussian modulation [37], we base our analysis on the security proofs for collective attacks under the trusted-device scenario described in [25]. The parameters required to evaluate the Holevo bound, computed according to [25], are determined during the parameter-estimation phase. The post-processing steps for methods ① to ③ are summarized in Fig. 8.

IV. RESULTS

To experimentally validate the findings on distance limitations associated with constant-rate FEC, we perform IR across a range of VOA_{CH} settings. The results for code rates $R_c = \{0.04, 0.06, 0.08, 0.1\}$, shown in Fig. 9, demonstrate that a positive extracted SKR is only achievable within distinct attenuation ranges or, equivalently, distance windows when converted to SSMF length. As exemplified for the $R_c = 0.06$ FEC code in Fig. 10, the FER rises significantly, approaching one, for attenuations larger than 5 dB. Conversely, for an attenuation less than 4.5 dB, the ratio χ_{EB}/R_c increases and eventually exceeds one, implying that Eve gains more information on the shared secret than Alice and Bob. Thus, secret key extraction using the $R_c = 0.06$ constant-rate FEC code is feasible only within the narrow attenuation range around 4.5 dB to 5 dB. Using a set of constant-rate FEC codes as in method ①, the VOA_{CH} attenuation ranges from approximately 2.5 dB to 4 dB, 4.5 dB to 5 dB and 6.5 dB to 7 dB can be covered with the investigated codes.

Although methods ① and ②, i.e., tuning modulation variance and adding controlled amounts of trusted detector loss, still rely on a single FEC code with fixed rate, they extend the operational range of the system. Figure 11 shows the

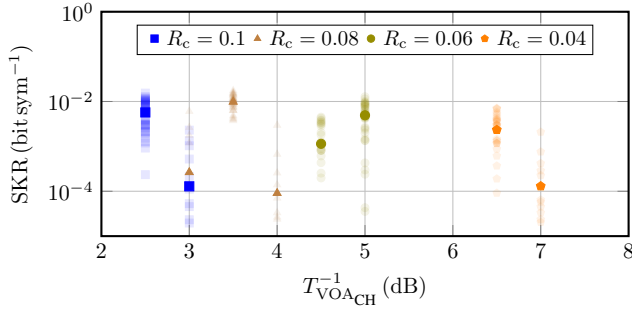


Fig. 9. Experimental results for method ① over the VOA_{CH} attenuation, considering only runs with non-negative excess noise. The means for each VOA_{CH} attenuation setting are indicated with solid markers.

extracted SKR for a constant code rate of $R_c = 0.06$, tuning modulation variance and trusted detector loss for distance-adaptivity. As illustrated, both approaches enable secure key extraction up to approximately 47.7 km of emulated fiber distance, corresponding to the VOA_{CH} setting of the considered experimental runs. Beyond this point, further adjustment of the trusted detector loss is no longer feasible, as it would imply an unphysical improvement of the detector efficiency. Under the given experimental conditions, continued scaling of the modulation variance enables the system to sustain a positive SKR up to 79 km of emulated fiber distance. Throughout tuning both parameters, their values remain within experimentally viable ranges, as shown in the inset of Fig. 11.

For method ③, we investigate the use of rate-adaptive error-correcting codes. The extracted SKR is shown in Fig. 12 for reconciliation efficiencies $\beta = \{0.93, 0.95, 0.97, 0.99\}$. As depicted, the rate-adaptive FEC codes with 93%, 95% and 97% reconciliation efficiency yield positive extracted SKRs across the entire range of considered attenuation settings. In contrast, the rate-adaptive FEC code with 99% reconciliation efficiency only allows for secret key extraction when the attenuation is larger than 0.5 dB and smaller than 10.5 dB. Although

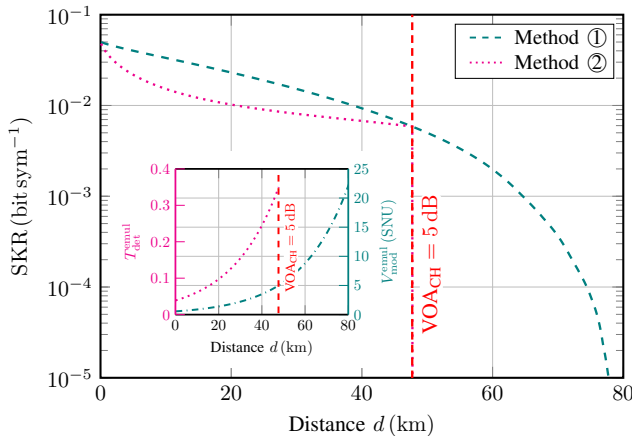


Fig. 11. Experimental results for methods ① and ② using an FEC code with rate $R_c = 0.06$ over the emulated fiber distance d . We take into account only experimental runs with non-negative excess noise, and compute the mean extracted SKR over the group of measurements with the same VOA_{CH} setting. The inset plot illustrates the tuned values of V_{mod} and T_{det} .

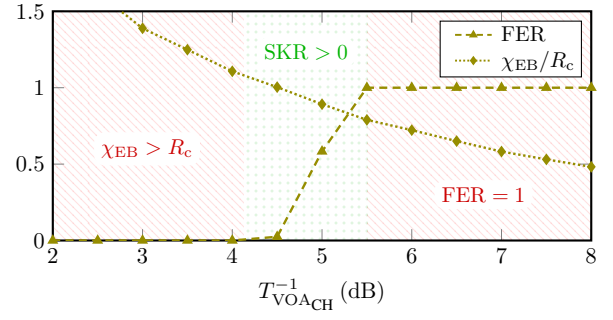


Fig. 10. Experimental results for method ① over the VOA_{CH} attenuation. We depict mean FER and mean fraction χ_{EB}/R_c using the $R_c = 0.06$ constant-rate FEC code for IR.

this configuration achieves the highest asymptotic SKR, i.e., $\beta I_{\text{AB}} - \chi_{\text{EB}}$, the extracted SKR experiences a severe penalty due to the high FER as illustrated in the inset of Fig. 12. Contrarily, the FER of the FEC code with $\beta = 0.93$ remains below an FER of 0.5 throughout all evaluated attenuation settings. Therefore, despite having the lowest asymptotic SKR among the examined rate-adaptive FEC codes, its reduced FER penalty outweighs the smaller asymptotic key rate, yielding the highest extracted SKR of all considered rate-adaptive FEC schemes. To maximize reach, the reconciliation efficiency should be chosen as large as possible, given that the FER is smaller than one, since it ultimately defines when the difference $\beta I_{\text{AB}} - \chi_{\text{EB}}$ becomes zero.

In Fig. 13, we present the performance of all investigated methods over emulated fiber distance. For the sake of a fair comparison and due to experimental limitations, we adjust the modulation variance of approaches using rate-adaptive FEC for distances below 20 km and beyond 80 km similar to approach ① by scaling the modulation variance according to (5). To determine the extracted SKR, we use the closest (in terms of distance) experimental results, i.e., the protocol runs at approximately 20 km and 80 km. As reference, we depict the

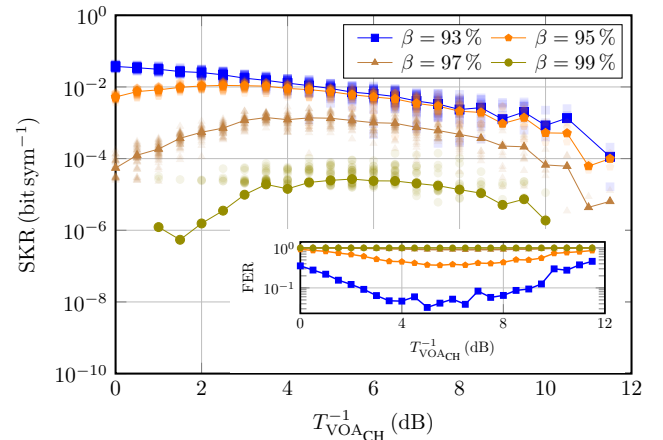


Fig. 12. Experimental results for method ③ considering different reconciliation efficiencies over the VOA_{CH} attenuation. Only protocol runs with positive excess noise are used for the computation of the extracted SKR. The mean extracted SKR for each attenuation setting is indicated with a solid marker. The inset plot depicts the average FER.

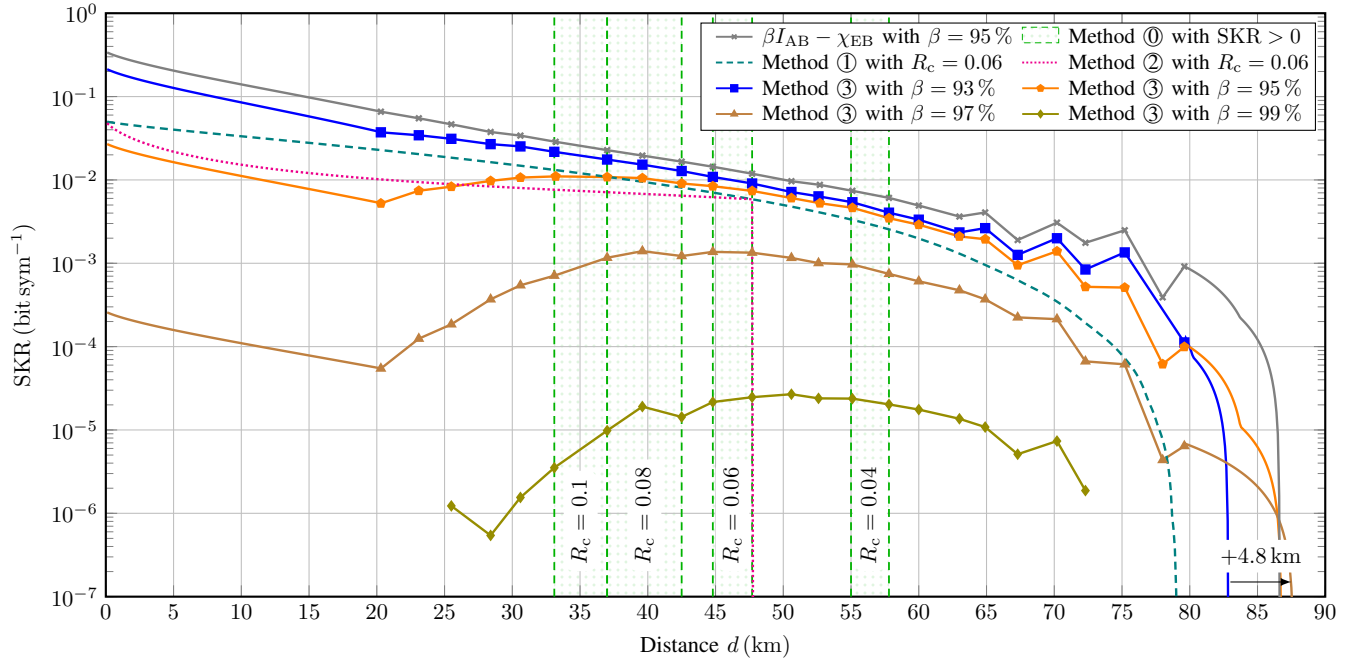


Fig. 13. Experimental results for mean extracted secret key rate over the emulated fiber distance d . We depict a reference curve, i.e., $\beta I_{AB} - \chi_{EB}$ with $\beta = 95\%$, and the four investigated approaches to distance-adaptivity. For all methods, we compute the extracted SKR only for experimental runs with non-negative excess noise.

asymptotic SKR, i.e., $\beta I_{AB} - \chi_{EB}$ for a fixed reconciliation efficiency of 95%. Effectively, this represents an ideal rate-adaptive error-correcting code with zero residual frame errors and distance-independent reconciliation efficiency.

Due to the discrete attenuation steps of the considered experimental setup, we depict the green-shaded distance regions for the FEC codes of method ① where positive extracted SKRs are obtained. As shown, the chosen constant-rate FEC codes are able to cover distance windows up to a maximum width of 5.5 km. Therefore, method ①, i.e., employing all four constant-rate FEC codes, is able to extract secrecy only for a small subset of considered distances. Covering the full distance range requires a considerably higher number of FEC codes since the distance windows become narrower for higher transmission distances.

When comparing methods ① and ②, both of which employ a single constant-rate FEC code, a performance penalty relative to the reference curve is observed. For method ①, the penalty is smaller than for method ②, reaching around one order of magnitude in SKR for the latter below 10 km. In addition, the secret key extraction of method ② is limited to distances smaller than 47.7 km, whereas tuning the modulation variance in method ① facilitates continuous operation up to 79 km. Since we keep the received SNR constant over distance by adjusting either the modulation variance or the trusted detector loss and the same FEC code is used, both methods achieve a distance-independent reconciliation efficiency of 95.96%. Therefore, at an emulated distance of 47.7 km, where the modulation variance and the trusted detector loss are the same for methods ① to ③, the extracted SKR lies in between those of the rate-adaptive method with $\beta = 95\%$ and $\beta = 97\%$.

Method ③, which employs rate-adaptive FEC, operates close to the reference curve for distances between 40 km and 70 km, where the FERs of the rate-adaptive FEC codes with reconciliation efficiencies of 93% and 95% are relatively small. Outside this range, the performance penalty increases, reaching roughly one order of magnitude for distances below 20 km when considering the FEC code with $\beta = 0.95$. In contrast, due to the significantly lower FER exhibited by the FEC code with $\beta = 0.93$, the gap between the (zero-FER) reference curve and the extracted SKR is substantially smaller. Using rate-adaptive FEC with higher reconciliation efficiencies allows for longer reach, but also introduces larger performance penalties for shorter distances. For instance, the rate-adaptive FEC code with 97% reconciliation efficiency achieves an additional 4.8 km transmission distance compared to the code with 93% reconciliation efficiency. However, this improvement comes at the expense of an SKR penalty of three orders of magnitude below 20 km of emulated fiber distance. Due to the high FER of the rate-adaptive FEC code with $\beta = 0.99$, it is only able to extract key material from 25.5 km to 72.3 km, being the narrowest distance window and featuring the lowest extracted SKR of methods ① to ③.

V. DISCUSSION

The inherent distance limitations associated with constant-rate FEC codes restrict the use of CV-QKD systems to small windows of consecutive distances. Using constant-rate FEC with a *single* code is viable only if the operating distance of the system is known in advance and falls within an operational distance window. As an alternative approach, a potentially extensive set of constant-rate FEC codes, each tailored to cover

a specific target distance window, could be used. However, implementing this approach necessitates numerous code designs and entails more hardware utilization since the parity-check matrices of all FEC codes need to be stored. In addition, even small variations in the received SNR during runtime can have a significant impact on the extracted SKR, especially when the system operates near the zero-key threshold. Therefore, using constant-rate FEC for IR is suboptimal without further adjustments.

Tuning the modulation variance or adding controlled amounts of trusted detector loss can enable distance-adaptive operation using a single constant-rate FEC code. With respect to implementation, methods ① and ② can be realized based on the information locally available to Alice and Bob. For method ①, the received SNR is known to Alice through IR. With this knowledge, Alice is able to adjust the modulation variance using VOA_{TX} . In method ②, Bob has access to the received SNR after parameter estimation and can therefore apply the correct amount of trusted detector loss by adjusting the attenuation of VOA_{RX} . Since both VOAs are essential to implement the CV-QKD protocol, i.e., either by attenuating the QKD signal to the quantum level or by implementing the shutter during calibration, there is no additional cost on hardware. If the accompanying SKR penalty is tolerable, these methods increase the operational range considerably and are a simple method to overcome the distance limitations otherwise imposed by constant-rate FEC. Due to the practical limitations in adjusting the trusted detector loss, tuning the modulation variance is better suited for long-distance CV-QKD.

When the reconciliation efficiency is selected appropriately, the rate-adaptive FEC utilized in method ③ achieves SKRs that approach the asymptotic reference curve. Unlike methods ① and ②, in which Alice or Bob need to modify parameters of the quantum transmission phase, method ③ requires no adjustments on the physical layer, thereby enabling joint optimization of protocol parameters and FEC. This benefit comes at the expense of additional complexity in the decoder implementation. Although a single decoder architecture is sufficient for RL-LDPC codes, selecting the appropriate subgraph corresponding to the given code rate increases the design complexity. Furthermore, the hierarchical decoder structure constrains the block lengths as lower-rate codes necessitate larger block lengths that cannot be independently configured. Therefore, choosing a specific code rate and block length also determines the block lengths of adjacent rates. As comparable requirements for rate-adaptive FEC exist in mobile networks, this class of decoders has undergone standardization for 5G NR [38].

To ensure a fair performance comparison of the analyzed methods, we performed IR on recorded measurement data. In a practical system, however, methods ① and ② can only be applied prior to the subsequent protocol run, not retroactively after a run has completed. Therefore, the temporal stability of the investigated CV-QKD system and its sensitivity to parameter changes are of particular interest to ensure that the adjusted parameters actually yield non-zero SKRs in the next protocol run. One possible realization to mitigate these shortcomings is to characterize the CV-QKD system

using an analytical model, and to implement a feedback loop between Alice and Bob to optimize the modulation variance as demonstrated in [18]. We expect that a similar method could also be applied to method ②. In contrast, since method ③ requires no changes on the physical layer, its application to a practical system is simpler as the code rate (or equivalently the reconciliation efficiency) can be chosen independently after the quantum transmission phase. It would therefore be better suited for free-space applications, as retrospective tuning of system parameters is not feasible due to rapidly varying channel conditions [35].

VI. CONCLUSION

In this work, we analyze the fundamental limitations of CV-QKD employing constant-rate FEC codes. Our analysis shows that a positive SKR can only be achieved within constraint distance windows where two conditions are fulfilled: (i) the FER is less than one, and (ii) the code rate is larger than the Holevo bound. By employing a set of constant-rate FEC codes, distance-adaptive operation can be realized, albeit at the cost of requiring numerous such codes. To overcome this limitation, we investigate three alternative strategies for distance-adaptive CV-QKD. The first two methods, i.e., tuning modulation variance or adding controlled amounts of trusted detector loss, can facilitate continuous operation without restrictive distance windows using a single constant-rate FEC code. With the investigated experimental setup, secret key extraction is possible up to 47.7 km when controlled amounts of trusted detector loss are added, or up to 79 km when the modulation variance is tuned. As an alternative, we study rate-adaptive FEC and find that operation near the asymptotic SKR can be achieved over a wide range of distances, provided that the trade-off between FER and reconciliation efficiency is selected appropriately. In future work, joint optimization of system parameters, such as modulation variance and trusted detector loss, in combination with rate-adaptive FEC could be explored experimentally to maximize the SKR and extend the reach of CV-QKD systems.

REFERENCES

- [1] J. Berl *et al.*, "Comparison of methods for distance-adaptive continuous-variable quantum key distribution," in *Proc. European Conference on Optical Communication (ECOC)*, 2024, pp. 27–30.
- [2] L. Gyongyosi and S. Imre, "A survey on quantum computing technology," *Computer Science Review*, vol. 31, pp. 51–71, 2019. DOI: 10.1016/j.cosrev.2018.11.002.
- [3] S. S. Gill *et al.*, "Quantum computing: A taxonomy, systematic review and future directions," *Software: Practice and Experience*, vol. 52, no. 1, pp. 66–114, 2022. DOI: 10.1002/spe.3039.
- [4] Z. Yang, M. Zolanvari, and R. Jain, "A survey of important issues in quantum computing and communications," *IEEE Communications Surveys & Tutorials*, vol. 25, no. 2, pp. 1059–1094, 2023. DOI: 10.1109/COMST.2023.3254481.
- [5] P. W. Shor, "Polynomial-time algorithms for prime factorization and discrete logarithms on a quantum computer," *SIAM Journal on Computing*, vol. 26, no. 5, pp. 1484–1509, 1997. DOI: 10.1137/S0097539795293172.
- [6] C. Gidney, *How to factor 2048 bit RSA integers with less than a million noisy qubits*, 2025. Preprint, arXiv: 2505.15917.
- [7] S. Pirandola *et al.*, "Advances in quantum cryptography," *Advances in Optics and Photonics*, vol. 12, no. 4, 2020. DOI: 10.1364/AOP.361502.
- [8] C. H. Bennett and G. Brassard, "Quantum cryptography: Public key distribution and coin tossing," *Theoretical Computer Science*, vol. 560, no. P1, pp. 7–11, 2014. DOI: 10.1016/j.tcs.2014.05.025.

- [9] F. Laudenbach *et al.*, “Continuous-variable quantum key distribution with Gaussian modulation – the theory of practical implementations,” *Advanced Quantum Technologies*, vol. 1, no. 1, 2018. DOI: 10.1002/qute.201800011.
- [10] V. Scarani *et al.*, “The security of practical quantum key distribution,” *Reviews of Modern Physics*, vol. 81, no. 3, pp. 1301–1350, 2009. DOI: 10.1103/RevModPhys.81.1301.
- [11] G. Zhang *et al.*, “An integrated silicon photonic chip platform for continuous-variable quantum key distribution,” *Nature Photonics*, vol. 13, no. 12, pp. 839–842, 2019. DOI: 10.1038/s41566-019-0504-5.
- [12] J. Aldama *et al.*, “Integrated QKD and QRNG photonic technologies,” *Journal of Lightwave Technology*, vol. 40, no. 23, pp. 7498–7517, 2022. DOI: 10.1109/JLT.2022.3218075.
- [13] A. A. E. Hajomer *et al.*, “Continuous-variable quantum key distribution at 10 GBaud using an integrated photonic-electronic receiver,” *Optica*, vol. 11, no. 9, pp. 1197–1204, 2024. DOI: 10.1364/OPTICA.530080.
- [14] M. Almeida *et al.*, “Secret key rate of multi-ring M-APSK continuous variable quantum key distribution,” *Optics Express*, vol. 29, no. 23, pp. 38 669–38 682, 2021. DOI: 10.1364/OE.439992.
- [15] F. Roumestan *et al.*, “Demonstration of probabilistic constellation shaping for continuous variable quantum key distribution,” in *Proc. Optical Fiber Communication Conference (OFC)*, 2021, F4E.1. DOI: 10.1364/OFC.2021.F4E.1.
- [16] Y. Pan *et al.*, “Experimental demonstration of high-rate discrete-modulated continuous-variable quantum key distribution system,” *Optics Letters*, vol. 47, no. 13, 2022. DOI: 10.1364/OL.456978.
- [17] D. Pereira *et al.*, “Probabilistic shaped 128-APSK CV-QKD transmission system over optical fibres,” *Optics Letters*, vol. 47, no. 15, pp. 3948–3951, 2022. DOI: 10.1364/OL.456333.
- [18] L. Ma *et al.*, “Practical continuous-variable quantum key distribution with feasible optimization parameters,” *Science China Information Sciences*, vol. 66, no. 8, 2023. DOI: 10.1007/s11432-022-3712-3.
- [19] M. Almeida, A. N. Pinto, and N. A. Silva, “Modulation variance optimization in discrete modulated CV-QKD systems,” in *Emerging Imaging and Sensing Technologies for Security and Defence VIII*, SPIE, 2023. DOI: 10.1117/12.2683577.
- [20] M. Almeida *et al.*, “Reconciliation efficiency impact on discrete modulated CV-QKD systems key rates,” *Journal of Lightwave Technology*, vol. 41, no. 19, pp. 6134–6141, 2023. DOI: 10.1109/JLT.2023.3280076.
- [21] S. Kreinberg, I. Koltchanov, and A. Richter, “Adding artificial noise for dynamic code rate matching in continuous-variable quantum key distribution,” in *Proc. Conference on Lasers and Electro-Optics (CLEO)*, 2020. DOI: 10.1364/CLEO_AT.2020.ATH11.6.
- [22] C. Zhou *et al.*, “Continuous-variable quantum key distribution with rateless reconciliation protocol,” *Physical Review Applied*, vol. 12, no. 5, 2019. DOI: 10.1103/PhysRevApplied.12.054013.
- [23] H. Yang *et al.*, “High-efficiency rate-adaptive reconciliation in continuous-variable quantum key distribution,” *Physical Review A*, vol. 109, no. 1, 2024. DOI: 10.1103/PhysRevA.109.012604.
- [24] C. E. Shannon, “A mathematical theory of communication,” *The Bell System Technical Journal*, vol. 27, no. 3, pp. 379–423, 1948. DOI: 10.1002/j.1538-7305.1948.tb01338.x.
- [25] F. Laudenbach and C. Pacher, “Analysis of the trusted-device scenario in continuous-variable quantum key distribution,” *Advanced Quantum Technologies*, vol. 2, no. 11, 2019. DOI: 10.1002/qute.201900055.
- [26] X. Wang *et al.*, “Efficient rate-adaptive reconciliation for continuous-variable quantum key distribution,” *Quantum Information and Computation*, vol. 17, 13&14 2018. DOI: 10.26421/QIC17.13-14.
- [27] C. Zhou *et al.*, “Rate compatible reconciliation for continuous-variable quantum key distribution using Raptor-like LDPC codes,” *Science China Physics, Mechanics & Astronomy*, vol. 64, no. 6, 2021. DOI: 10.1007/s11433-021-1688-4.
- [28] E. E. Cil and L. Schmalen, “Rate-adaptive protograph-based Raptor-like LDPC code for continuous-variable quantum key distribution,” in *Proc. Advanced Photonic Congress: Signal Processing in Photonic Communications (SPPCom)*, 2024, JTU1A.51. DOI: 10.1364/BGPP.2024.JTU1A.51.
- [29] F. Roumestan *et al.*, “Shaped constellation continuous variable quantum key distribution: Concepts, methods and experimental validation,” *Journal of Lightwave Technology*, vol. 42, no. 15, pp. 5182–5189, 2024. DOI: 10.1109/JLT.2024.3391168.
- [30] S. Kleis, M. Rückmann, and C. Schäffer, “Continuous variable quantum key distribution with a real local oscillator using simultaneous pilot signals,” *Optics Letters*, vol. 42, no. 8, pp. 1588–1591, 2017. DOI: 10.1364/OL.42.001588.
- [31] F. Laudenbach *et al.*, “Pilot-assisted intradyne reception for high-speed continuous-variable quantum key distribution with true local oscillator,” *Quantum*, vol. 3, p. 193, 2019. DOI: 10.22331/q-2019-10-07-193.
- [32] H.-M. Chin *et al.*, “Digital synchronization for continuous-variable quantum key distribution,” *Quantum Science and Technology*, vol. 7, no. 4, 2022. DOI: 10.1088/2058-9565/ac7ba2.
- [33] A. Leverrier *et al.*, “Multidimensional reconciliation for a continuous-variable quantum key distribution,” *Physical Review A - Atomic, Molecular, and Optical Physics*, vol. 77, no. 4, 2008. DOI: 10.1103/PhysRevA.77.042325.
- [34] E. E. Cil and L. Schmalen, *An open-source library for information reconciliation in continuous-variable QKD*, 2024. arXiv: 2408.00569. Available (commit: edf3450b): https://github.com/erdemera/IR_for_CVQKD.
- [35] K. Gümüş *et al.*, “Rate-adaptive reconciliation for experimental continuous-variable quantum key distribution with discrete modulation over a free-space optical link,” *Journal of Lightwave Technology*, vol. 43, no. 8, pp. 3564–3573, 2025. DOI: 10.1109/JLT.2025.3530005.
- [36] L. E. Dickson, “On quaternions and their generalization and the history of the eight square theorem,” *Annals of Mathematics*, vol. 20, no. 3, pp. 155–171, 1919.
- [37] A. Denys, P. Brown, and A. Leverrier, “Explicit asymptotic secret key rate of continuous-variable quantum key distribution with an arbitrary modulation,” *Quantum*, vol. 5, p. 540, 2021. DOI: 10.22331/q-2021-09-13-540.
- [38] T. Richardson and S. Kudekar, “Design of low-density parity check codes for 5G new radio,” *IEEE Communications Magazine*, vol. 56, no. 3, pp. 28–34, 2018. DOI: 10.1109/MCOM.2018.1700839.